

# Moment Preserving Constrained Resampling with Applications to Particle-in-Cell Methods

D. Faghihi<sup>1</sup>, V. Carey<sup>3</sup>, C. Michoski<sup>2</sup>, R. Hager<sup>4</sup>, S. Janhunen<sup>2</sup>, C. S. Chang<sup>4</sup>,  
and R. D. Moser<sup>2</sup>

<sup>1</sup>Department of Mechanical and Aerospace Engineering, University at Buffalo

<sup>2</sup>Oden Institute for Computational Engineering and Sciences, University of Texas at Austin

<sup>3</sup>Department of Mathematics and Statistics, University of Colorado Denver

<sup>4</sup>Princeton Plasma Physics Laboratory, Princeton NJ

February 13, 2020

## Abstract

The Moment Preserving Constrained Resampling (MPCR) algorithm for particle resampling is introduced and applied to particle-in-cell (PIC) methods to increase simulation accuracy, reduce compute cost, and/or avoid numerical instabilities. The general algorithm partitions the system space into smaller subsets and resamples the distribution within each subset. Further, the algorithm is designed to conserve any number of particle and grid moments with a high degree of accuracy (i.e. machine accuracy). The effectiveness of MPCR is demonstrated with several numerical tests, including a use-case study in gyrokinetic fusion plasma simulations. The computational cost of MPCR is negligible compared to the cost of particle evolution in PIC methods, and the tests demonstrate that periodic particle resampling yields a significant improvement in the accuracy and stability of the results.

*Keywords:* Particle-in-cell, particle resampling, distribution function moments, constrained optimization.

## 1 Introduction

Particle-in-cell (PIC) methods are a class of numerical techniques for solving partial differential equations using a mixed Lagrangian (particle) and Eulerian (grid cell) representation. Here we consider PIC methods applied to systems described by the evolution of the characteristics of a distribution function  $f$ . An obvious example is Boltzmann's equation for the distribution of atomic or molecular particles in physical and velocity

space for a thermodynamic system. Application of PIC methods is particularly natural for the solution of Boltzmann’s equation in plasmas because the mean electromagnetic interaction of the charged atomic particles is easily described through the Eulerian representation of electromagnetic fields on a spatial grid. For this reason, PIC methods have been widely used in plasma simulations [1, 2, 3], both to solve the Boltzmann equations (including atomic particle collisions) or the Vlasov equations (neglecting atomic particle collisions). It is this application of PIC methods to plasma simulation that motivated the current work, but the resampling algorithms are applicable to any **sampled** representation of a distribution function.

In the PIC methods considered here, the marker particles that represent the distribution function  $f$  do so in a Monte Carlo sense; that is, the marker particles are considered a random sample drawn from the distribution  $f$ . In this way, expected values and conditional expectations defined from  $f$  are simply computed as averages or conditional averages over the marker particles. While these “Monte Carlo PIC” methods are simple and easy to implement, they suffer from sampling error, which reduces slowly (like  $N^{-1/2}$ ) as the number of marker particles  $N$  increases. More complex, higher-order PIC methods [4, 5] have also been developed. They converge more rapidly through the use of a deterministic Lagrangian representation of  $f$ , but they also require frequent remapping of the marker particles representing  $f$ . Here, we pursue Monte Carlo PIC (just PIC from now on) for its simplicity, and consider resampling algorithms to ensure that it is as accurate as possible for a given number of particles.

A particle-in-cell method is useful because the Lagrangian particle motion is a natural representation of the evolution of the distribution function  $f$ , given the field quantities (e.g. the electromagnetic fields in plasmas) that determine the particle motion, while the fields are determined from  $f$  (e.g. the charge and current densities in plasmas). Thus, one of the defining features of a PIC method is that information carried by the particles must be projected onto the grid, where it is needed for the Eulerian solution of the field quantities using finite difference [6], finite volume [7], and/or finite element [8] discretizations. Another defining feature is that the field quantities represented on the grid must be interpolated to the particle locations to determine the particle evolution. A third feature of the PIC methods discussed here is that since the particles are samples of the distribution function  $f$ , they are not the same as physical particles; rather they are often called marker particles, macro-particles, or sometimes superparticles. For example, the marker particles are not atomic particles even when  $f$  is an atomic particle distribution; indeed, there are generally many orders of magnitude fewer marker particles than atomic particles in a system. These PIC features, particularly the projection of particle information onto the grid, drive some of the requirements for the resampling algorithms described here.

In Monte Carlo sampling of a distribution function  $f$ , one is often concerned that low-probability (small- $f$ ) regions of the phase space distribution may not be well represented, because there will be very few particles in this region. For example, in plasma simulations, an accurate representation may be needed of the physics in low plasma

density regions of space, or high kinetic energy regions of velocity space. To accomplish this, importance sampling is often employed [9, 10], in which more samples are taken in low probability regions, and the samples are weighted accordingly. In this case, expectations on  $f$  are computed as weighted averages over the particles.

In a plasma PIC simulation, for example, an accurate representation of the physics throughout the physical domain may dictate that the marker particles be evenly distributed throughout physical space, with variable weights representing the variation of plasma density in space. There may be similar requirements in velocity space. However, as  $f$  evolves in time, there will be mixing of marker particles that spoils the desired marker particle distribution, degrading the representation of  $f$ , and thus the accuracy of the simulation. Furthermore, in some PIC methods, to reduce the number of particles and increase the accuracy, a control variate approach is used [11, 12, 13], in which the difference between  $f$  and some reference distribution  $f_0$  is represented through marker particle sampling. In these  $\delta f$  methods, the particle weights evolve, which can lead to sample degeneration in which the weights become concentrated on just a few particles as the simulation proceeds; resulting in a poor representation of the distribution. This phenomena is similar to the sample degeneracy observed in particle filtering methods [14, 15, 16, 17, 18, 19, 20].

For all of these reasons, it is important that the marker particle distributions in a PIC simulation be periodically adjusted to maintain the required importance sampled marker particle distribution. In doing this resampling, there are conserved physical quantities (e.g. mass, momentum, energy, angular momentum) that should be preserved throughout the process. Further the projection of quantities on to the grid, such as charge and current in a plasma simulation, should also be preserved through the resampling. In this way, there will be no change in the field quantities as a result of the resampling.

Many methods for particle resampling that preserve various moments or distributional features of the solution have been explored. Many of these methods rely on splitting and merging the original particles and are capable of preserving a limited number of derived features (e.g. moments) to some degree of accuracy. For example, Lapenta [21, 22, 23] proposed a scheme in which the number of particles is increased by splitting particles and decreased by coalescence of particles close to each other in phase space. The algorithm is applicable to PIC simulations with two-dimensional and three-dimensional Cartesian grids and can preserve overall charge, momentum, and energy. However, this algorithm cannot conserve other features of the velocity distribution function, and the scheme is not directly extendable to 2D or 3D unstructured grids. Teunissen and Ebert [24] improved Lapenta's particle merging algorithm using the k-d tree method to search for the nearest neighbor. Following a similar procedure, Vranic et al. [25] divided the momentum space into smaller cells for sorting particles that resulted in better local preservation of the energy, momentum, and charge.

A different two-dimensional method of coalescing particles in PIC methods that conserves the particle and cell charge and current densities, as well as the particle en-

ergy, is presented by Assous [26]. However, the method is limited to two-dimensional triangular cells and its extension to other cell geometries and three-dimensions is not straightforward. Moreover, in this method the number of particles per cell after coalescence is restricted depending on the integration points employed in the solution. Welch et al. [27] provided an extension of Assous method [26] to coalescing particles on 2D and 3D cells. This method is limited to orthogonal grids and is similar to the method of Assous, in that coalescence might not be possible in some cases.

Luu et al. [28] presented a particle merging algorithm in which the phase space of a simulation is partitioned into smaller subsets. The algorithm merges particles that are close to each other and provides direct control over errors introduced by a merging event. Examining the performance of this algorithm indicates that momentum is conserved perfectly while energy conservation is approximate.

Pfeiffer et al. [29] proposed two algorithms for particle splitting and merging that use a 3D unstructured hexahedral mesh and are expandable to any cell geometry. The first method is computationally feasible and enables preserving particle charges, currents, and energies exactly, while the grid projected charge and current are only preserved approximately. The second method makes fewer assumptions about the velocity distribution function resulting in better conservation of the grid quantities, but is computationally more expensive.

In the work described here, we develop a general algorithm called Moment Preserving Constrained Resampling (MPCR) for resampling particles in a PIC simulation, while preserving any desired features of the distribution. The MPCR algorithm differs from the techniques described above by using the fact that the marker particles are a sampling representation of an underlying distribution  $f$ , and that this distribution can therefore be resampled when convenient. To accomplish this, MPCR uses a binning strategy based on any convenient discretization of phase space, making it suitable for general geometries and mesh/grid representations. It uses constrained optimization techniques to produce a new set of particle positions, velocities and weights that preserves any necessary (conditional) expectations on  $f$ , including physically conserved quantities and grid projections, to roundoff error.

The MPCR resampling algorithms described here can be applied to any problem in which PIC methods are used to represent the evolution of distributions. But, in this work, the target is a PIC representation of plasmas, particularly the simulation of edge physics in tokamak plasmas where particle resampling is most valuable due to the mixing of marker particles across strong plasma gradients. More specifically, the target in this case is the gyrokinetic PIC representation used in the XGC tokamak simulation codes [30, 31]. Details of the MPCR algorithm and its implementation in XGC are described in section 2. A number of example problems demonstrating the capabilities of MPCR are presented in section 3, and concluding remarks are provided in section 4.

## 2 Particle Resampling Strategies and Implementation

In this section, the proposed particle resampling algorithm is introduced, beginning with the constraints imposed on the resampled distribution (section 2.1), followed by the resampling process (section 2.2). Finally, as an example, a description of the implementation of the algorithm for use with the gyrokinetic code XGC is provided in section 2.3.

### 2.1 Resampling constraints

In the resampling process, we start with a representation of  $f$  by a set of  $N^p$  samples (particles) with specific positions, velocities and weights, and produce a new representation of  $f$  using a new set of  $M^p$  samples. In generating the new samples, it is important that physically relevant characteristics of the distribution function be preserved. These include physically important moments of  $f$ , as well as the coupling quantities that are projected from the particle representation to the grid. The general resampling strategy proposed here allows these quantities to be preserved to high accuracy. As an example, we consider here a set of constraints that are relevant to a PIC plasma simulation in which  $f(\mathbf{x}, \mathbf{v}, t)$  represents the atomic particle distribution in physical space ( $\mathbf{x}$ ) and velocity space ( $\mathbf{v}$ ). In other PIC applications, different constraints would be appropriate.

First, there are several velocity space moments that are physically relevant as functions of physical space. Among these are the atomic particle number density  $n$ , the momentum density  $\mathbf{m}$ , the kinetic energy density  $K$  and the momentum flux tensor (stress tensor)  $T$ .

$$n(\mathbf{x}, t) = \int f(\mathbf{x}, \mathbf{v}, t) d\mathbf{v}, \quad (1)$$

$$\mathbf{m}(\mathbf{x}, t) = m \int \mathbf{v} f(\mathbf{x}, \mathbf{v}, t) d\mathbf{v}, \quad (2)$$

$$K(\mathbf{x}, t) = \frac{1}{2} m \int |\mathbf{v}|^2 f(\mathbf{x}, \mathbf{v}, t) d\mathbf{v}, \quad (3)$$

$$T_{kl}(\mathbf{x}, t) = m \int v_k v_l f(\mathbf{x}, \mathbf{v}, t) d\mathbf{v}, \quad (4)$$

where  $m$  is the mass of the atomic particles represented by  $f$ , and in (4), Cartesian tensor notation is used. Preserving some or all of these quantities during resampling avoids introducing non-physical disruptions into the simulation caused by changes in these quantities. There are other velocity space moments, which, depending on the specific application, might also be important. For example, in gyrokinetic tokamak plasma simulations, it is often the canonical angular momentum that is relevant, rather than  $\mathbf{m}$ . All of these velocity space moments are functions of  $\mathbf{x}$ , and preserving them as continuous functions of  $\mathbf{x}$  will not be possible. Instead, they will be preserved in a discrete sense (see section 2.2), and in a global sense; that is, the integral over

the  $\mathbf{x}$  domain will be preserved. These correspond to global conservation of mass, momentum and energy. In addition, in some applications, it might be beneficial to preserve configuration space moments (i.e. moments taken with respect to  $\mathbf{x}$ ).

For a PIC plasma simulation, the charge density  $\rho$  and current density  $\mathbf{J}$  are needed as a function of  $\mathbf{x}$  to determine the electromagnetic fields. These are given trivially by  $\rho = qn$  and  $\mathbf{J} = q\mathbf{m}/m$ , where  $q$  is the charge of the atomic particles represented by  $f$ . However, what is important to the calculation is the representation of  $\rho$  and  $\mathbf{J}$  on the physical space grid. Consider the projection of a function of  $g(\mathbf{x})$  on to the discrete degrees of freedom (e.g. grid point values) defined by

$$g_j = \int \mathcal{P}_j(\mathbf{x})g(\mathbf{x}) d\mathbf{x} \quad (5)$$

where  $g_j$  is the discrete value for the  $j$ th degree of freedom, and  $\mathcal{P}_j$  is the projection kernel or shape function, which depends on the numerical methods employed on the Eulerian grid. In this case, the discrete values of the charge and current densities  $\rho_j$  and  $\mathbf{J}_j$  are given by:

$$\rho_j(t) = \int \int q\mathcal{P}_j(\mathbf{x})f(\mathbf{x}, \mathbf{v}, t) d\mathbf{v} d\mathbf{x}, \quad (6)$$

$$\mathbf{J}_j(t) = \int \int q\mathcal{P}_j(\mathbf{x})\mathbf{v}f(\mathbf{x}, \mathbf{v}, t) d\mathbf{v} d\mathbf{x}. \quad (7)$$

To ensure consistency of the electromagnetic fields computed from  $\rho$  and  $\mathbf{J}$  after the resampling, these grid projections need to be preserved.

## 2.2 The resampling algorithm

To generate a new sample of the distributions function  $f$  from an existing function, the MPCR algorithm begins by discretizing the sample phase space into bins. The resampling is then done independently in each bin, and the moments that are to be preserved are imposed as a constraint on the resampling in each bin. This approach has several benefits: 1) any non-ideal or local features of  $f$  (e.g. multi-modality or non-equilibrium peaks) will be preserved as long as they are resolved by the binning; 2) spatially dependent velocity moment constraints such as (1-4) and velocity dependent configuration moment constraints will be satisfied at the level of the binning discretization; 3) because the global characteristics of the distribution are resolved by the binning, the sampling performed on each bin can be simple, such as sampling from a uniform distribution on the bin, with weight adjustments to impose constraints; and finally 4) imposing the moment constraints will be performed as a constrained optimization, and by doing this on a bin-by-bin basis one reduces the dimension of each optimization problem. The details of the algorithm are described below, again using the case of a kinetic plasma PIC simulation as an example.

**Discretizing the phase-space.** The distribution function  $f$  is a function in the six dimensional physical and velocity space  $\zeta = (\mathbf{x}, \mathbf{v})$ . The algorithm begins by discretizing this six-dimensional space into bins, with each bin defining a volume in the  $\zeta$  domain. Each of the  $N^p$  particles is a sample of the distribution  $f$ , and so defines a point in the six-dimensional  $\zeta$  space, with a given weight. The particles are sorted into the bins according to their  $\zeta$  coordinate. The result is that the  $N^p$  particles are distributed among  $N^b$  bins, with bin  $i$  containing  $N_i^p$  particles. Depending on the application, it may be convenient to use the spatial discretization of the grid solver to define the bins. However, the MPCR can accommodate any bin geometry.

**Defining the number of new particles in each bin.** Recall, that the purpose of the resampling is to redistribute the marker particles in  $\zeta$  space to preserve the desired importance sampling, and if necessary increase or decrease the total number of particles. The desired importance sampled marker particle distribution can be defined as  $g(\zeta)$  where  $\int_{\zeta} g d\zeta = M^p$  is the target number of particles after resampling. Thus, the target number of new particles  $M_i^p$  in bin  $i$  is given by:

$$M_i^p = \int_{\zeta^i} g d\zeta, \quad (8)$$

where  $\zeta^i$  is the phase space domain of bin  $i$ , i.e. the range of position and velocity coordinates in the bin.

**Generating the new samples** In the  $i$ th bin, the target number of new samples  $M_i^p$  may be larger or smaller than the old number of samples  $N_i^p$ . If  $M_i^p \ll N_i^p$  and the variation of the weights among the old particles is not too great, it is advantageous to draw the  $M_i^p$  new particles as samples from the old particles. In this case, we use weighted sampling without replacement [32] in which a sample in a discrete population has a relative probability to be selected according to its weight and, once selected, is removed from the population. This method enables drawing  $M_i^p$  new samples while precluding the possibility of an old particle being sampled multiple times. This is important when the subsequent particle evolution is deterministic. Provided that  $M_i^p/N_i^p$  is sufficiently small compared to  $\text{avg}_j(w_j^i)/\max_j(w_j^i)$ , where  $w_j^i$  is the weight of the  $j$ th particle in bin  $i$ , the probability of  $M_i^p$  random draws from the old weighted particle distribution including any particle more than once is small. When this is so, uniformly weighted samples obtained using the sampling without replacement algorithm approach an unbiased sample from  $f$  on the bin, which is what makes this approach advantageous.

When this condition is not satisfied, a completely new set of  $M_i^p$  particles is sampled from a convenient distribution on the bin domain  $\zeta^i$ . A uniform distribution on  $\zeta^i$  is used here because it is the maximum entropy distribution supported in an interval (i.e., bin), and has the advantage of being simple. A maximum entropy distribution

constrained by some or all of the moment constraints is another possibility, but with sufficiently small bins this is of little value while being significantly more complicated.

**Imposing constraints** Within the bin, the weights of the new particles are intended to be uniform. There are two reasons for this. First, when the new particles are sampled from the old particles, the uniformly weighted particles approach a sampling of  $f$ . Second, for a given number of samples, uniformly weighted samples provide the most information about the distribution. However, in general, regardless of how the new samples are drawn, the samples will not satisfy the constraints as described in section 2.1. To impose these constraints, the weights are adjusted, while keeping them as close to uniform as possible through a constrained optimization.

To impose the constraints, the moment integrals are first restricted to the bin domain and then evaluated as a sum over the samples. For example, the bin restricted momentum from (2) is given by

$$\mathbf{m}^i = m \int_{\zeta^i} \mathbf{v} f(\zeta) d\zeta \approx m \sum_{j=1}^{N_i^p} \mathbf{v}_j^i w_j^i \quad (9)$$

where  $\mathbf{m}^i$  is the average momentum in bin  $i$  and  $\mathbf{v}_j^i$  is the velocity of particle  $j$  in bin  $i$ . Similar approximations of bin-wise atomic particle count  $n^i$ , kinetic energy  $K^i$  and momentum flux tensor  $T_{kl}^i$  can easily be written from equations (1–4). The objective is to ensure that these bin-wise quantities are the same when computed with the new samples as with the old samples. In addition, we impose similar constraints on the first and second configuration moments, primarily to improve the accuracy of the representation of  $f$  on the bin. The constraints to be imposed through adjustment of the weights  $\tilde{w}_j^i$  on the new particles are thus:

$$\sum_{j=1}^{M_i^p} \tilde{w}_j^i = \sum_{j=1}^{N_i^p} w_j^i, \quad (10)$$

$$\sum_{j=1}^{M_i^p} \tilde{\zeta}_j^i \tilde{w}_j^i = \sum_{j=1}^{N_i^p} \zeta_j^i w_j^i, \quad (11)$$

$$\sum_{j=1}^{M_i^p} (\tilde{x}_k \tilde{x}_l)_j^i \tilde{w}_j^i = \sum_{j=1}^{N_i^p} (x_k x_l)_j^i w_j^i, \quad (12)$$

$$\sum_{j=1}^{M_i^p} (\tilde{v}_k \tilde{v}_l)_j^i \tilde{w}_j^i = \sum_{j=1}^{N_i^p} (v_k v_l)_j^i w_j^i, \quad (13)$$

where  $\tilde{\zeta}_j^i$ ,  $\tilde{\mathbf{x}}_j^i$  and  $\tilde{\mathbf{v}}_j^i$  are the values of  $\zeta$ ,  $\mathbf{x}$  and  $\mathbf{v}$  for  $j$ th new particle in bin  $i$ . Thus, in addition to preserving the physical quantities  $n^i$ ,  $\mathbf{m}^i$ ,  $K^i$  and  $T_{kl}^i$  as a consequence



of (10) - (13), the conservation of moments in configuration space,  $\int \mathbf{x}f(\mathbf{x}, \mathbf{v}, t)d\mathbf{x}$  and  $\int \mathbf{x}^2f(\mathbf{x}, \mathbf{v}, t)d\mathbf{x}$ , lead to a better bin-wise representation of  $f$

Similarly, the grid projection quantities (charge and current densities in the plasma example) can be defined bin-wise, and the projection integrals as approximated by the sampling of  $f$  preserved through the resampling. For example, the current density projection (7) can be defined bin-wise as:

$$\mathbf{J}_m^i = q \int_{\zeta^i} \mathcal{P}_m(\mathbf{x})\mathbf{v}f(\zeta) d\zeta \approx q \sum_{j=1}^{N_i^p} \mathcal{P}_m(\mathbf{x}_j^i)\mathbf{v}_j^i w_j^i, \quad (14)$$

for each  $m$  for which bin  $i$  intersects the support of  $\mathcal{P}_m$ . Here  $\mathbf{J}_m^i$  is the contribution of bin  $i$  to degree of freedom  $m$  of the grid representation of the current. Therefore to preserve the grid projection of charge and current density, the following constraints are imposed:

$$\sum_{j=1}^{M_i^p} \mathcal{P}_m(\tilde{\mathbf{x}}_j^i)\tilde{w}_j^i = \sum_{j=1}^{N_i^p} \mathcal{P}_m(\mathbf{x}_j^i)w_j^i \quad \forall m \ni \text{bin}_i \cap \text{supp}(\mathcal{P}_m) \neq \emptyset \quad (15)$$

$$\sum_{j=1}^{M_i^p} \mathcal{P}_m(\tilde{\mathbf{x}}_j^i)\tilde{\mathbf{v}}_j^i\tilde{w}_j^i = \sum_{j=1}^{N_i^p} \mathcal{P}_m(\mathbf{x}_j^i)\mathbf{v}_j^i w_j^i \quad \forall m \ni \text{bin}_i \cap \text{supp}(\mathcal{P}_m) \neq \emptyset \quad (16)$$

where  $\text{bin}_i$  is the configuration space domain of bin  $i$ .

The weights  $\tilde{w}_j^i$  in the new sample can now be set to ensure that the constraints (10-13) and (15-16) are satisfied, while minimizing the variance in the weights by solving the following optimization problem:

$$\{\tilde{w}_j^i\}_{(j \in 1, 2, \dots, M_i^p)} = \arg \min_{\tilde{w}_j^i \in \mathcal{C}^i, \tilde{w}_j^i > 0} \sum_{j=1}^{M_i^p} (\bar{w}^i - \tilde{w}_j^i)^2, \quad (17)$$

where

$$\bar{w}^i = \frac{1}{M_i^p} \sum_{j=1}^{M_i^p} \tilde{w}_j^i, \quad (18)$$

and  $\mathcal{C}^i$  is the set of  $\tilde{w}^i$  satisfying the constraints (10-16). Notice that with a quadratic objective function (17) and linear equality constraints in  $\tilde{w}_j^i$  (10-16), this is a straightforward quadratic programming problem, for which efficient and well established algorithms are available [33].

**Comments, Remarks, and Discussion** The algorithm described here yields a resampling of the distribution  $f$  by discretizing the phase space into bins, with the assumption that  $f$  will then vary little over each bin. That is, that the binning provides

an accurate discrete representation of  $f$ . Clearly, the smaller the bin size, the more accurately the binning can represent  $f$ , but also the fewer particles will be in each bin. However, the number of particles in each bin must be greater than the number of constraints to be imposed during the resampling, preferably significantly greater. There is therefore a potential tradeoff in accuracy between decreasing bin size and increasing the number of constraints (e.g. imposing constraints on higher order moments), which is similar to the tradeoff between decreasing element size and increasing element order in finite element methods. In practice, as discussed in §2.3, the configuration space is binned according to the underlying spatial grid cells, and velocity space has been binned on a (typically)  $32 \times 32$  rectangular array. An adaptive approach to determining adequate bin sizes based on estimates of the resampling error (e.g. in unconstrained moments) may be useful.

The constrained optimization to minimize weight variances within a bin, as expressed in (17), is similar in formulation to the use of the *principle of maximum uniformity* proposed by Lapenta & Brackbill [23]. However, because here we are concerned with a sample-based representation of a distribution function ( $f$ ), the motivation is quite different. By minimizing the variance of the particle weights, we ensure that the particles carry near-maximum information about the distribution; whereas, in [23], the objective is to ensure a smooth representation of a continuous field. The motivation here is more closely related to the use of uniformly weighted samples in Monte Carlo methods.

In some particle evolution models, such as  $\delta f$  formulations as described in section 1, the particle weights must evolve. This can lead to sample degeneration in which weights become concentrated on fewer and fewer particles as the simulation proceeds, resulting in a poor distributional representation. Minimizing particle weight variance (17) in the optimization step of the resampling algorithm alleviates this degeneracy. As in particle filtering methods, maintaining relatively uniform particle weights improves the representation of the distribution, see e.g. [34].

MPCR has three notable features compared to recently developed particle splitting/merging algorithms in the PIC simulation context:

1. The sampling strategies used to define new particle distributions is easily applied to bins with irregular geometries, including, for example, unstructured meshes. This enables straight forward integration of the algorithm in any available PIC code. Moreover, since the optimization problems solved on each bin are independent, the computations at the bin level can be easily parallelized or built into the parallel solver of the PIC code.
2. As will be shown in the numerical results section, the constrained optimization technique is able to conserve any number of particle and grid quantities to *near machine precision* regardless of the method employed in the PIC code for particle evolution and deposition. Some of the previously developed algorithms in the literature [22, 35, 36] are successful in preserving some quantities but fail to

preserve grid projections or other characteristics of the distribution function. For example, the particle merging algorithm developed by Luu et al. [28] preserves total energy to only  $10^{-3}$ . In addition, the statistical particle split and merge methods recently proposed by Pfeiffer et al. [29], preserve grid projections to machine precision (or as reported to  $10^{-19}$ ) for the low-order cell mean projection, but is much less accurate (only  $10^{-2}$ ) for higher order grid projections.

3. The bin-wise constrained optimization used in the resampling algorithm can introduce a subtle parallel inefficiency. The problem arises when there are too few particles in a bin to satisfy all the constraints. This is easily addressed by merging neighboring bins until there are enough particles in the merged bin. This merging process disrupts the parallel efficiency of the optimization calculations. This is not a serious concern because resampling is done infrequently, so that the cost of resampling including the extra cost of bin merging, is small compared to time evolving the PIC simulation. Marker particle weight distributions can be used to adaptively determine when resampling is necessary.

### 2.3 Implementation in the XGC gyrokinetic PIC code

MPCR can be applied to resample any distribution function, but as an example application we apply it here to a gyrokinetic plasma PIC code. In this section, we describe the XGC gyrokinetic PIC codes for tokamak fusion reactor simulations [37, 38] along with specific implementation issues for integrating MPCR.

The time evolution of plasma systems is described by the six dimensional Maxwell-Boltzmann system in phase space [39]. In strongly magnetized plasmas, such as tokamak fusion plasmas, these equations can be averaged analytically over the gyrophase (viz. the cyclotron frequency) leading to a gyrocenter tracking equation for a charged ring that evolves with the relatively slow motion of particle gyrocenters. This treats rapid particle orbits about magnetic field lines asymptotically. Transforming to the gyrocenter coordinate then results in a phase space reduction from six to five dimensions, and the resulting system of equations is referred to as the gyrokinetic equations. While a significant simplification is achieved through the reduction of the full six-dimensional equations to five-dimensional gyrokinetic equations [3], simulating this five-dimensional system in a full-scale tokamak fusion reactor is still a formidable task requiring a carefully formulated numerical scheme and large-scale high-performance computers.

The Lagrangian evolution equations for the marker particle positions, velocities and weights depend on exactly how  $f$  is sampled. In a straight-forward approach (called full- $f$ ), the distribution is simply sampled. However, this requires the largest number of particles to accurately represent  $f$ , and is therefore computationally most expensive. Other algorithms use a control-variate ( $\delta f$ ) approach in which the difference between  $f$  and an ideal or simple distribution  $f_0$  is sampled. There are a number of such  $\delta f$  approaches that differ in the details; see for example [40]. In the full- $f$  representation, the particle weights do not evolve in time, but in  $\delta f$  approaches, they do. The details

of a resampling algorithm for a full- $f$  and  $\delta f$  sampling scheme may differ, because of the difference in representation. In the algorithm described here, we consider a full- $f$  sampling representation of  $f$  for simplicity.

The XGC code-base supports a large collection of PIC solution strategies, allowing for full- $f$ , delta- $f$ , and total- $f$  (or equivalently, hybrid-Lagrangian [40]) simulations, where in each case the XGC PIC algorithms support turbulence over a plasma volume parameterized in a toroidal reactor geometry, following the magnetic axis across the magnetic separatrix and scrape-off layer (SOL), to just outside the sheath interfacing material boundary. The XGC PIC model uses a cylindrical coordinate system, in which the components of the particle position vector are  $\mathbf{x} = (r, z, \phi)$ , and the velocity vector  $\mathbf{v}$  decomposes into parallel and perpendicular components along the magnetic field  $\mathbf{B}(r, z, \phi)$  via projections  $v_{\parallel} = \mathbf{v} \cdot \mathbf{B}/|\mathbf{B}|$  and  $v_{\perp} = |\mathbf{v} - v_{\parallel}\mathbf{B}/|\mathbf{B}|$ . The code propagates marker particles using Lagrangian motion and the corresponding fields are solved on a finite element mesh. Due to the need to represent irregular material boundaries and the magnetic X-point, XGC uses a 2D unstructured triangular mesh [41]. A constraint imposed on the mesh is that nodes must lie on magnetic flux surfaces of constant  $\psi$  (see Fig. 1), which also acts as an effective radial coordinate for 1D diagnostics.

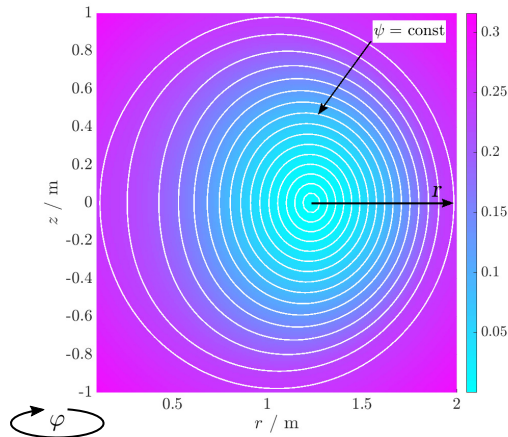


Figure 1: Equipotentials of the flux function  $\psi$ , along with the cylindrical coordinate axes used in the XGC code.

Integrating MPCR into the XGC PIC algorithm begins with the Eulerian spatial discretization, which is based on unstructured triangular meshes in planes of constant  $\phi$ . In XGC, for the purpose of parallel computation, the particles are sorted into specific sub-volumes of the domain defined through the mesh, and we use these volumes as the configuration-space MPCR bins to avoid additional parallel communication. These volumes are defined by considering the two-dimensional  $r$ - $z$  mesh at the points in  $\phi$  that are half-way between the constant- $\phi$  planes of the Eulerian grid. The plane is tiled into

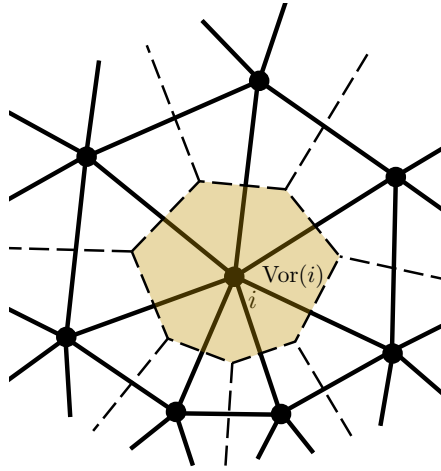


Figure 2: Illustration of a 2D unstructured mesh and Voronoi cell associated with the vertex (node)  $i$ . The finite element nodes and elements are represented by points and solid lines. The dashed lines indicate the Voronoi cells.

*Voronoi cells* around each vertex of the two-dimensional mesh, as shown in figure 2. The binning volumes are then defined as the extrusion of the Voronoi cells along the magnetic field lines to the closest constant- $\phi$  planes of the grid. Sorting into these Voronoi bins effectively groups together the particles closest to the same constant- $\phi$  mid-plane whose projection along the field lines onto that mid-plane is closest to the same mesh vertex [42]. In the MPCR algorithm, the particles in each Voronoi bin are further sorted into uniformly spaced Cartesian bins in the two-dimensional gyrokinetic velocity space  $\mathbf{v} = (v_{\parallel}, v_{\perp})$ , and moment-constrained resampling is performed on each Voronoi/Cartesian bin.

The resampling constraints include both simple moment constraints such as (10)-(13) and the grid-projection constraints (15)-(16). The definition of the moment constraints is straight-forward, and the operators  $\mathcal{P}_m$  in the grid-projection constraints are defined based on the numerical operators used in XGC to project the particle information onto the Eulerian grid. Specifically, the Eulerian degrees of freedom  $m$  are defined on the vertices of the three-dimensional grid, which is more naturally enumerated by the index  $k$  of the vertex on the two-dimensional triangular mesh, and the index  $l$  of the constant- $\phi$  grid plane. For any point in configuration space  $\mathbf{x}$ , let  $\Delta^+(\mathbf{x})$  be the mesh triangle in which the magnetic field line through  $\mathbf{x}$  intersects the closest grid plane in the positive  $\phi$  direction, enumerate this grid plane as  $l^+(\mathbf{x})$ , and let  $\text{Vert}(\Delta^+(\mathbf{x}))$  be the set of three vertices of  $\Delta^+(\mathbf{x})$ . Further, let  $\lambda_k^+(\mathbf{x})$  for  $k \in \text{Vert}(\Delta^+(\mathbf{x}))$  be the barycentric coordinate in  $\Delta^+(\mathbf{x})$  associate with vertex  $k$  of the magnetic field line projection of  $\mathbf{x}$ . Finally let  $\beta^+(\mathbf{x})$  be the distance along the field line from  $\mathbf{x}$  to plane  $l^+(\mathbf{x})$  normalized by distance along the field line from plane  $l^+(\mathbf{x})$  to plane  $l^-(\mathbf{x})$ , which is the closest constant- $\phi$  plane to  $\mathbf{x}$  in the negative  $\phi$  direction. Similarly  $\Delta^-$ ,  $\lambda_k^-$  and  $\beta^-$

are the same for the grid plane  $l^-(\mathbf{x})$ . Note that  $\beta^+(\mathbf{x}) + \beta^-(\mathbf{x}) = 1$  and  $\sum_k \lambda_k^\pm = 1$ , where the sum is over  $k \in \text{Vert}(\Delta^\pm(\mathbf{x}))$ . Then the grid projection operator  $\mathcal{P}_{k,l}(\mathbf{x})$  is given by

$$\mathcal{P}_{k,l}(\mathbf{x}) = \begin{cases} \beta^+(\mathbf{x})\lambda_k^+(\mathbf{x}) & \text{if } k \in \text{Vert}(\Delta^+(\mathbf{x})) \text{ and } l = l^+(\mathbf{x}) \\ \beta^-(\mathbf{x})\lambda_k^-(\mathbf{x}) & \text{if } k \in \text{Vert}(\Delta^-(\mathbf{x})) \text{ and } l = l^-(\mathbf{x}) \\ 0 & \text{otherwise} \end{cases} \quad (19)$$

This then completes the definition of the charge and current grid-projection constraints in (15)-(16).

### 3 Numerical Examples

In this section we present several numerical examples motivated by the use of MPCR in full- $f$  gyrokinetic simulations. In these examples, the constrained optimization problem (17) is solved using the well-established algorithm of Goldfarb & Idnani [43] as implemented in the *quadprog* library [44]. There are numerous other optimization algorithms that could be used for this straight-forward quadratic programming problem.

In the first set of test problems, we demonstrate the ability of MPCR to preserve features of the distribution function when resampling an arbitrary distribution and resampling particles from an XGC plasma turbulence solution. Finally we show the benefits of periodic particle resampling using MPCR on a neoclassical tokamak plasma simulation. In a neoclassical simulation, transport is represented by a diffusion process that is formulated to account for the effects of the magnetic geometry, which may produce complex particle orbits and drifts.

In addition to the tests reported here, the resampling algorithm was applied to Landau damping simulations to ensure that resampling preserves the phase-space structure of the solution, as expected it does. However, Landau damping is not a compelling case for the use of the resampling algorithm described here because it does not require strong particle weight variations. It will therefore not be considered further here. This is in contrast to *remapping* algorithms applicable to a different class of PIC methods as described by [5], which have the objective of preserving the placement of computational particles on a Cartesian mesh in physical and velocity space, and which *are* of value in the Landau damping problem.

#### 3.1 Global resampling examples

For the first example, consider the one-dimensional probability distribution represented by the histogram shown in Figure 3(a). It might, for example, be a distorted marginal distribution of one of the velocity components. In this case, Maxwell-Boltzmann statistics would yield a Gaussian distribution, and the given distribution is clearly far from Gaussian. In this figure, the synthetic distribution function  $f$  is presented as a function of a general phase space variable  $\alpha$ , which could, for example, be any velocity or position coordinate of the phase space. This distribution is represented with  $N^p = 50000$

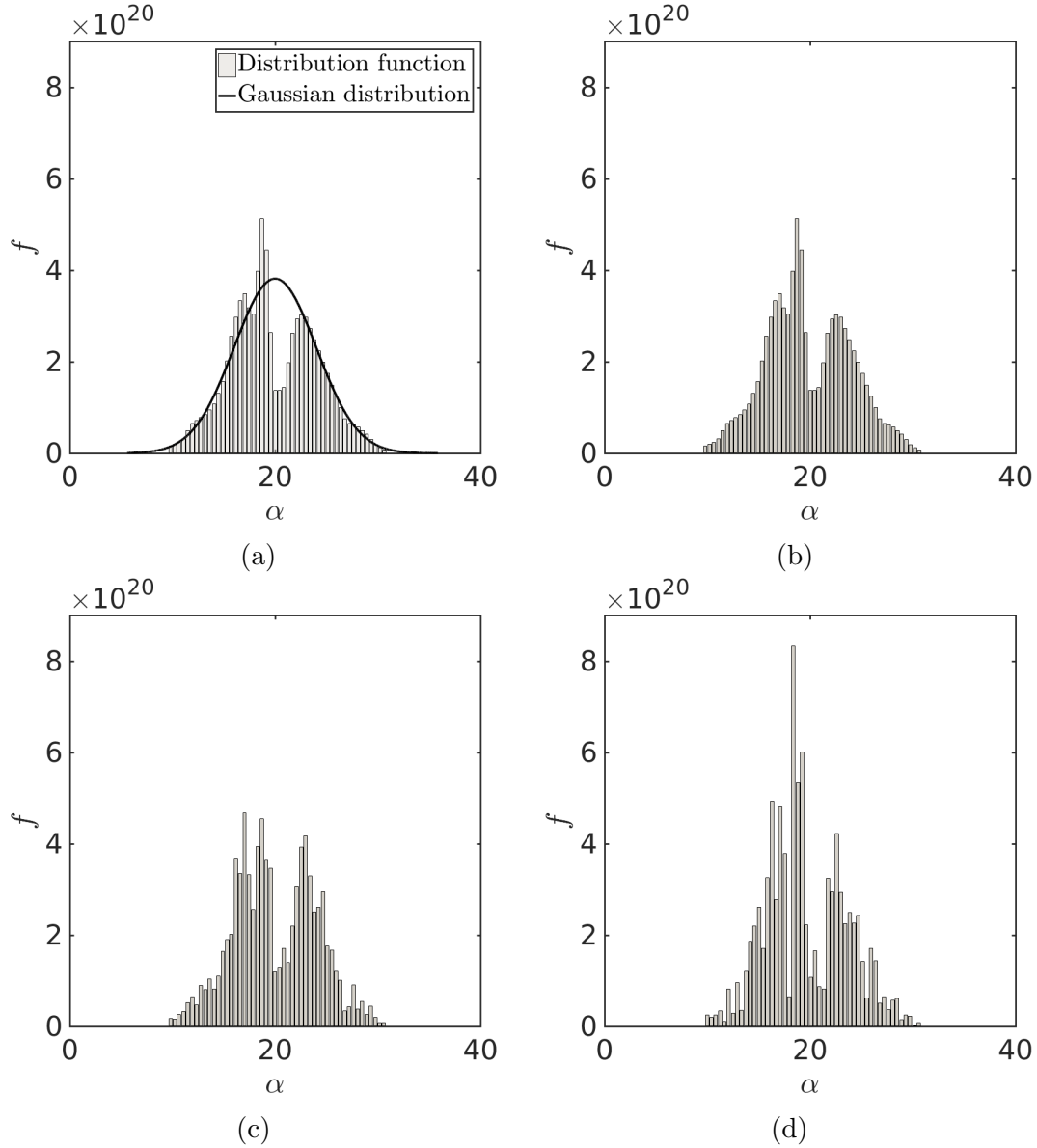


Figure 3: Synthetic distribution  $f$  as a function of general phase space variable  $\alpha$ , as represented initially by  $N^p = 50000$  marker particles, and down-sampled by a factor 50 and 200, using MPCR and global random down-sampling. The MPCR algorithm is applied with 50 bins, which are the same as the bins used in the histograms. Shown are: (a) initial distribution, (b) MPCR with  $\text{DSF} = 200$ , and global random down-sampling with (c)  $\text{DSF} = 50$  and (d)  $\text{DSF} = 200$ . In (a), the curve is a Gaussian.

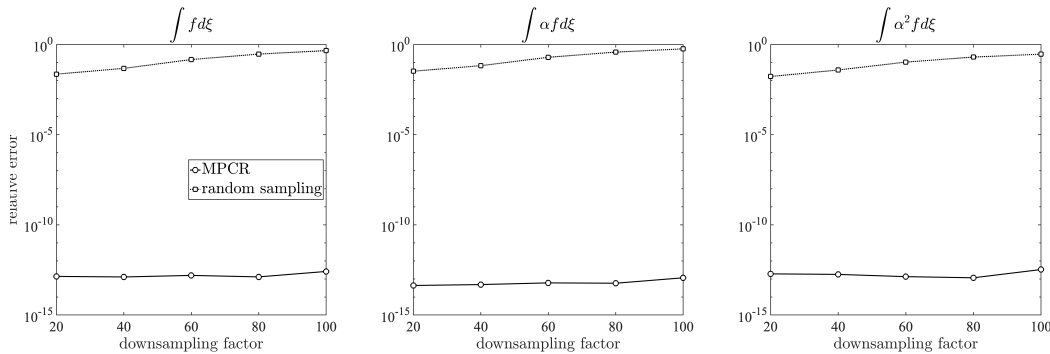


Figure 4: Relative error in global zeroth, first, and second moments due to feature-based/random down-sampling for different down-sampling factors (error in random down-sampling is the mean of  $10^4$  realizations).

samples with non-uniform weights generated from a perturbed Gaussian, and down-sampled to  $M^p = 1000$  and  $M^p = 250$ : down-sampling factors (DSF) of 50 and 200, respectively.

Down-sampling was performed using MPCR in one-dimension, using  $M^b = 50$  bins in which the sample density, and first and second moments are preserved. For comparison, global random down-sampling was also used, in which  $M^p$  new marker particles are selected randomly from the  $N^p$  old particles. Such global down-sampling has been used in the past in plasma PIC codes, for example, in the XGC plasma simulation codes. The results are shown in Figures 3 and 4. By construction, the histogram formed on the 50 down-sampling bins is identical to that of the original sample, but the randomly down-sampled histograms show large variations from the original. Indeed, the sampling error obscures the structure of the distribution; so much so that in the DSF=200 case, the underlying structure of the distribution is not visible at all. By construction, the low-order moments of the distribution are preserved in MPCR, as shown in Figure 4, whereas relative errors in the moments with random down-sampling range from 2% to 10%.

MPCR up-sampling was also tested on the distribution function from Figure 3(a), with similar results. That is, constrained moments are preserved to roundoff error, while detailed features of the distribution are preserved on the scale of the binning (not shown). A common alternative up-sampling approach is particle reproduction [17], in which each particle is duplicated  $n_u$  times, where  $n_u$  is the up-sampling factor. This will obviously preserve all moments and all features of the sampled distribution function. However, if the subsequent evolution of the particles in the PIC code is deterministic, it will accomplish nothing, since the particles will remain identical for all time and not provide an improved sample of  $f$ . To avoid this, some algorithms perturb the position and/or the velocity of the duplicated particles [17], which without further adjustment results in the target moments not being preserved. As the duplicated and perturbed



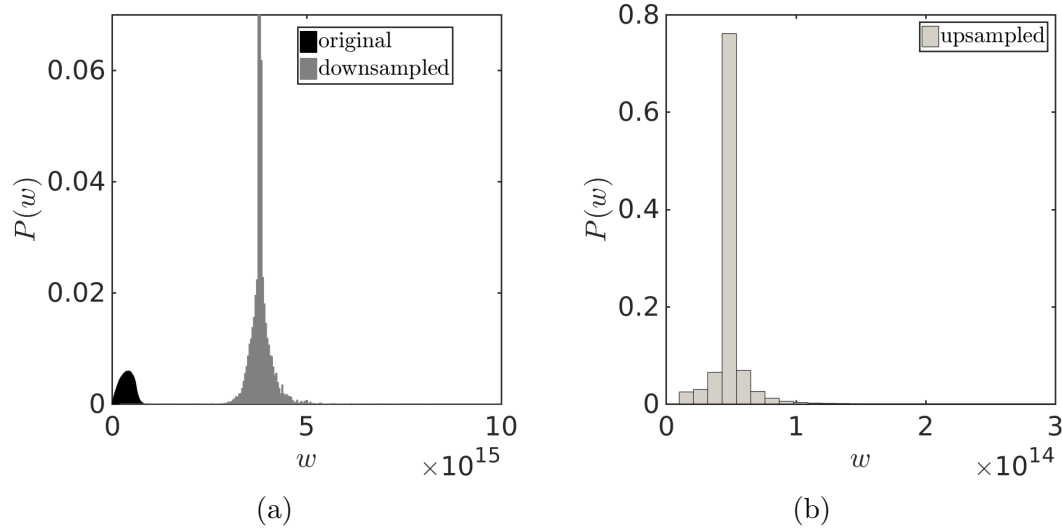


Figure 5: Histograms of particle weights from the original weights and the proposed resampling algorithm. In this case  $N^p = 10^6$  and the number of bins in the  $\rho$ ,  $\mu$ ,  $r$  and  $z$  directions is 50: (a) original particles and downsampled particles with down-sampling factor (DSF) = 20, (b) upsampled particles with up-sampling factor (USF) = 10.

particles evolve, they will commonly diverge from one-another (assuming the particle evolution is chaotic), and become independent samples of the distribution after some time, with the divergence rate governing how long this takes. Similarly, if particle evolution is stochastic, then exactly duplicated particles will also diverge, and also become independent samples of the distribution over time. In contrast, by sampling from a binned approximation of  $f$  and imposing a set of integral constraints, MPCR up-sampling produces nearly independent samples immediately.

For a second example, the resampling algorithm is applied to the particle distribution taken from a tokamak plasma simulation performed with the gyrokinetic PIC code XGC1. In a spatially three-dimensional gyrokinetic PIC code, each particle is characterized by six attributes, its weight  $w$ , spatial coordinates  $\mathbf{x} = (r; z; \phi)$ , and velocity coordinate  $\mathbf{v} = (v_{\parallel}; v_{\perp})$ . In this example, the distribution  $f$  is projected on to a spatially two-dimensional configuration space in  $r$  and  $z$ , taking advantage of statistical homogeneity in  $\phi$ . The motivation for this aspect of the test, is to enable the projection of a solution from a spatially three-dimensional plasma turbulence simulation to serve as an initial condition for a two-dimensional neoclassical simulation. The data set consists of  $N^p = 10^6$  particles, initially weighted to effect importance sampling, as discussed in Section 2. However, particles have since been mixed through their evolution, so their weights no longer accomplish the desired importance sampling.

The first step of the particle resampling process is to divide the four-dimensional phase space  $\zeta$  into bins and sort the particles into those bins. In the gyrocentered XGC1

code, the particle velocity space is parameterized in terms of the normalized parallel velocity  $\rho = v_{\parallel}/B$  and magnetic moment  $\mu = v_{\perp}^2/2B$ , where  $B$  is the magnitude of the magnetic field. For this case then, the four-dimensional down-sampled phase space is  $\zeta = (r, z, \rho, \mu)$ . The  $\zeta$  domain is divided into bins, with 50 bins in each of the four phase-space directions.

To demonstrate the adjustment of weights as part of the resampling process the importance weighting is eliminated by making  $g \propto f$ , where  $g$  is the marker particle distribution function in (8) to enforce uniform target weights in bins. The target number of particles  $M_i^p$  in each bin is then simply proportional to the sum of the weights of the original particles in the bin. Specifically,

$$M_i^p = M^p \left( \frac{\sum_{j=1}^{N_i^p} w_j^i}{\sum_{j=1}^{N^p} w_j} \right). \quad (20)$$

One complication that arises in sorting the particles into bins is that in some cases the target number of down-sampled particles  $M_i^p$  in a bin is too small to allow the constraints to be imposed. In this case, neighboring bins in the velocity space directions  $(\rho, \mu)$  are merged to form larger bins with more particles, until  $M_i^p$  exceeds a specified minimum, which was set here to  $M_i^p \geq 25$ .

The distribution of particle weights is shown in Figure 5 for the original particles, and for the result of down-, and up-sampling using the MPCR algorithm. Note that the original distribution is broad, while the resampled distributions are strongly peaked. The target marker particle distribution for both cases was to eliminate importance sampling and make the weights uniform. The fact that the resampled weight distributions are not delta-functions is a consequence of the weight adjustments used to preserve moments. The down-sampled particle weights are much larger than the original weights and the up-sampled weights are much smaller because the mean of the weights must increase (decrease) by the down-scaling (up-scaling) factor. Also by construction, the features of the distribution in both space and velocity are preserved after resampling.

The accuracy of the moment preservation in the resampling approach is tested by down-sampling while preserving different moments. Three cases were considered: preserving 1) the zeroth moment, 2) the zeroth and first moments, and 3) the zeroth through second moments, as described in Section 2. This was done for a range of down-sampling factors, and resulting errors in the moments are shown in Figures 6, along with errors for random down-sampling. The moment errors for the random down-sampling are averaged over  $10^4$  sampling realizations.

There are several interesting features of these errors. First, as expected, the relative errors in the moments that are preserved are order  $10^{-10}$  or less. Second, with the MPCR algorithm, even the moments that are not constrained have significantly lower errors than for random sampling, in some cases by three orders of magnitude. This improvement over random sampling is presumably due to the binning, which enforces

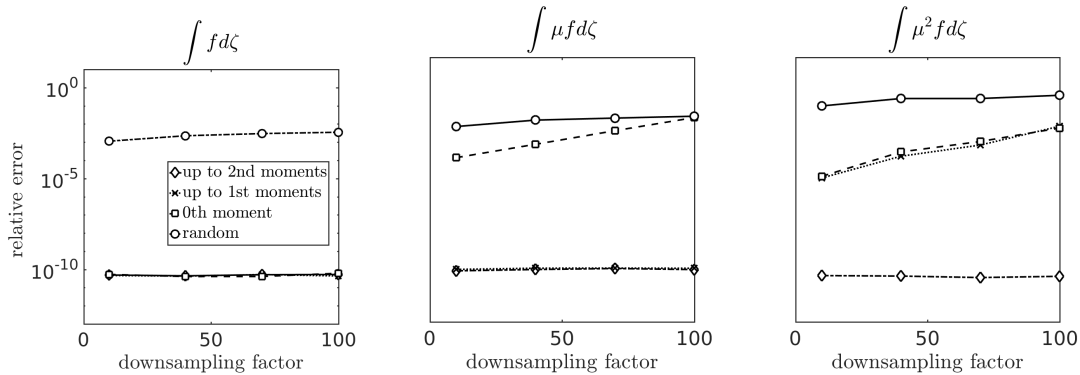


Figure 6: Relative error in global zeroth, first and second velocity space moments as a function of down-sampling factor, using random down-sampling and MPCR down-sampling constrained to preserve zeroth, up to first and up to second moments. Errors in configuration space moments are similar. There were  $N^p = 10^6$  original particles extracted from XGC1, and there were 10 bins in the  $\rho$ ,  $\mu$ ,  $r$  and  $z$  directions, for a total of  $10^4$  bins.

a discrete representation of the global distribution that defines the moments. Notice in particular that the error in the second moment when constraining the first moment is only marginally better than when just the zeroth moment is constrained. Finally, for both random down sampling and for unconstrained moments in MPCR, the relative error increases with down-sampling factor. The observed weak growth is as expected for random sampling, which should introduce errors that scale with the square root of the down-sampling factor. In contrast the relative errors in the unconstrained moments in MPCR grow much more rapidly with down-sampling factor.

The reduction of errors relative to random down-sampling due to binning, as discussed above, suggests that in MPCR, moment errors should reduce with increasing bin density. This is indeed the case, as shown in Figure 7, where relative error in an up-sampling case is plotted as a function of the number of bins in each direction. The error in the first moment when only the zeroth moment is constrained appears to be decreasing like the number of bins in each direction squared. Recall that the up-sampling algorithm involves sampling a uniform distribution on each bin. As mentioned in Section 2, more sophisticated sampling in each bin can be used, which could result in a more rapid reduction of errors with number of bins. Finally note that as with down-sampling, preserved moments have relative errors that are better than  $10^{-10}$ .

### 3.2 Periodic particle resampling of a neo-classical PIC simulation

In this subsection, we apply the MPCR algorithm to tokamak plasma test cases using the XGCa code. For context, the code and simulation characteristics are described

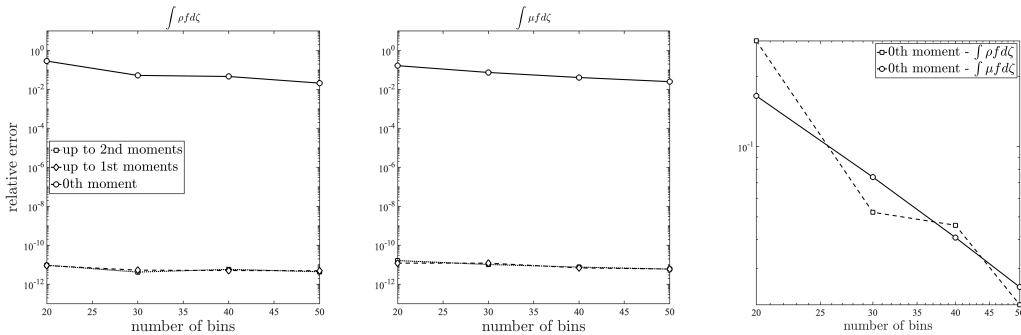


Figure 7: Relative error in global first moments in  $\rho$  and  $\mu$  as a function of the number of bins in each direction,  $\rho$ ,  $\mu$ ,  $r$  and  $z$ . MPCR up-sampling was used, constrained to preserve zeroth, up to first and up to second moments. There were  $N^p = 10^6$  original particles extracted from XGC1, and the up-scaling factor was 10.  $E(\mu) \approx N^{-2.1}$  and  $E(\rho) \approx N^{-2.7}$ , where  $N$  is the number of bins and  $E(\cdot)$  is the error in the corresponding moment.

briefly below, before presentation of simulation results. XGCa [45, 46, 31] is a global gyrokinetic particle-in-cell (PIC) code with an axisymmetric electrostatic potential solver specialized for the simulation of neoclassical transport physics in the edge plasma of toroidal magnetic confinement devices. These simulations are capable of evolving the full five-dimensional gyrocenter distribution function from the magnetic axis to the inner wall of the device using either conventional full- $f$  (constant particle weight) [31] or total- $f$  (variable particle weights) [46] methods.

As a proof-of-principle test, the impact of the MPCR algorithm on several important characteristics of the simulated plasma are investigated here; particularly the radial electric field that is needed to maintain quasi-neutrality, the maintenance of a divergence-free equilibrium plasma flow, and the conservation of toroidal angular momentum. For simplicity, we use the full- $f$  representation of a single ion species (deuterium) with the adiabatic electron model.

The magnetic equilibrium field is that of a generic, up-down symmetric, low-aspect ratio tokamak with a circular boundary surface and Shafranov shift. Marker particles are initiated with a uniform distribution in configuration and velocity space and perpendicular and parallel velocities of up to approximately  $3.5v_{th}$ , where  $v_{th}$  is the thermal velocity. The marker particle weights  $w$  are set to produce a locally Maxwellian distribution with density  $n_i(\psi)$  and temperature  $T_i(\psi)$  that depend only on the flux-label (generalized minor radial coordinate)  $\psi$ ; that is, each particle's initial weight is a function of its initial flux-label and velocity. The electrostatic potential is initially zero.

A local Maxwellian is, however, not the neoclassical equilibrium distribution in the presence of a pressure gradient, due to the magnetic inhomogeneity drift, which

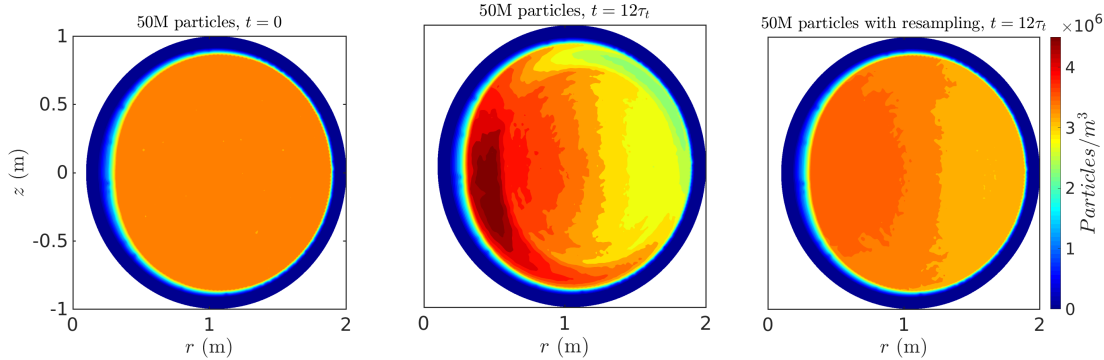


Figure 8: Spatial distribution of particle density for the simulation with 50 million particles: initial particle distribution (left), at  $t = 12\tau_t$  without resampling (middle), and at  $t = 12\tau_t$  with resampling (right).

causes charged particles in tokamaks to move on so-called banana-orbits with finite width. Starting with a local Maxwellian distribution and vanishing radial electric field, the orbital motion of the ions, together with the background pressure gradient leads to the development of an up-down anti-symmetric pressure variation and a net toroidal flow. If this were the equilibrium flow it would violate the divergence-free condition and toroidal angular momentum conservation. To make the equilibrium flow divergence free and cancel the net toroidal flow from the magnetic inhomogeneity drift, the plasma reacts by generating a radial electric field (guiding center polarization) with its corresponding  $\mathbf{E} \times \mathbf{B}$  flow.

The challenge in calculating the radial electric field with a full-f PIC code arises because the orbital motion of the markers leads to mixing of particles with disparate weights. This is a considerable source of sampling error, especially in regions with small pressure gradient and low amplitude of the electrostatic potential. The purpose of periodic particle-resampling is to reduce the sampling error by locally homogenizing the particle weights and by improving the distribution of marker particles in phase space. We demonstrate this capability by comparing the time evolution of the radial electric field and the radial electric field profile in quasi-steady state between simulations with a total of 5 million, 50 million, and 500 million marker particles without particle re-sampling, and a simulation with 50 million particles with periodic resampling.

In all cases, the PIC simulations are run for 12 toroidal transit times ( $\tau_t$ ), which is sufficient for the equilibrium plasma flow to develop, and in this case the toroidally averaged equilibrium solution is expected to be slowly varying with no temporal oscillations. The spatial marker particle density is intended to be approximately uniform through the core and edge plasma to yield a good representation of the low-density edge region. However, as the plasma evolves the particles mix and the initial marker distribution becomes inhomogeneous, spoiling the intended importance sampling. This is apparent in Figure 8, in which the initial and final marker particle densities for the

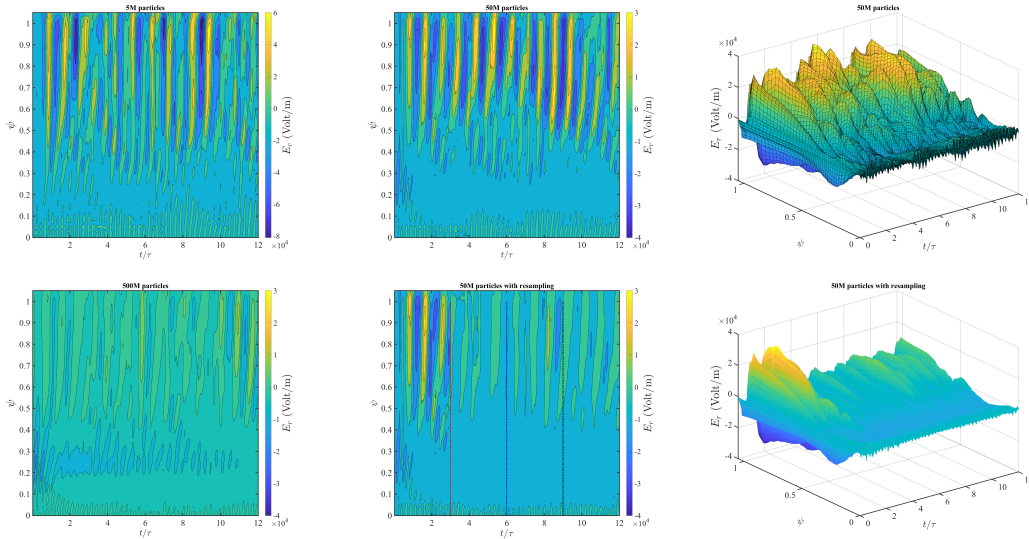


Figure 9: Spatio-temporal evolution of  $E_r$  in simulations with 5, 50 and 500 million particles without resampling and 50 million particles with resampling.

50 million particle case are plotted (no resampling). A similar mixing occurs in velocity space, which would spoil any importance sampling used, for example, to represent high energy ions. The result of this poor sampling of the particle distribution is that large Monte Carlo sampling error is introduced into the simulation. As an example, consider the spatio-temporal evolution of the radial electric field (Figure 9) for the 5, 50 and 500 million particle cases (no resampling). In all three cases, there are spurious oscillations, which are largest in the edge region,  $0.8 < \psi < 1$ , because the marker particle densities are low in this region. Further, the magnitude of these oscillations is reduced with increasing number of particles. Particularly, the oscillation magnitude decreased by about a factor of  $\sqrt{10}$  going from 50M and 500M particles, which is the expected asymptotic convergence rate for errors dominated by sampling error.

To reduce the sampling error, the MPCR algorithm was applied periodically in the 50 million particle simulation, in this case every 3 toroidal transit times ( $3\tau_t$ ). There are 1500 time steps between resamples, and the computational cost of resampling is negligible compared to the time advance for this number of steps. As described in Section 2.3, the 2-dimensional unstructured mesh in XGC consists of 6368 elements, and in velocity space 100 uniform bins were used in both the  $v_{\parallel}$  and  $v_{\perp}$  directions. At each resampling, the total number of marker particles remained the same ( $M^p = N^p$ ), and the target number of particles in each bin is consistent with the initial marker particle distribution (at  $t = 0$ ).

As a result of the periodic resampling, the marker particle distribution in configuration space at the end of the simulation is much more uniform than without the resampling (Figure 8). This leads to much smaller oscillations in the radial electric

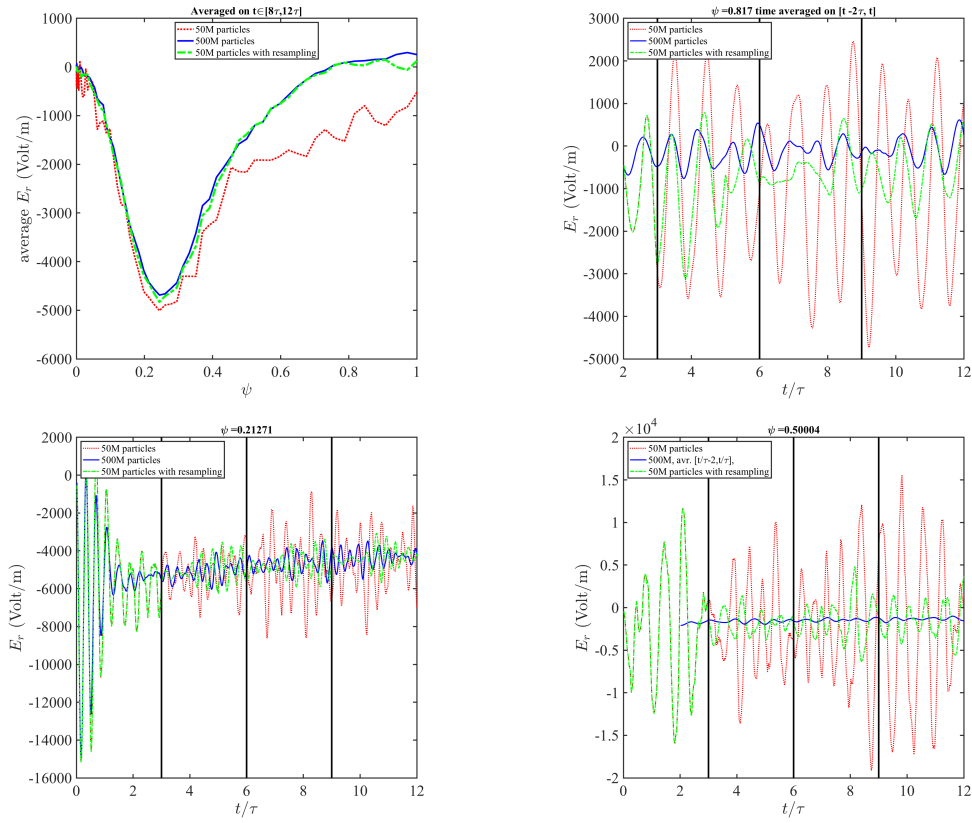


Figure 10:  $E_r$  profile at  $t = 12\tau_t$  and Time evolution of  $E_r$  at  $\psi = 0.5$ ,  $\psi = 0.2$ ,  $\psi = 0.8$ , for simulations with 50 million particles with and without resampling, and 50 million particles. Resampling occurs at the times marked with a vertical black line.

field  $E_r$  (see Figure 9). The resampled and non-resampled cases are identical until the first resampling at  $t = 3\tau_t$ . After the resampling the spurious oscillations in  $E_r$  are immediately reduced. Indeed, it is reduced to levels comparable to the 500M particle non-resampled case, as can be seen in Figure 10 where the time evolution of  $E_r$  at several points in  $\psi$  is plotted for the both 50 million particles cases (resampled and not) and the 500 million particle case. Also shown is the  $E_r$  profile as a function of  $\psi$  averaged over the period  $8\tau_t < t < 12\tau_t$ , and the profile from the 50 million particle resampled case is a much more accurate approximation of the 500 million particle profile than the non-resampled case. As an indicator of the oscillations in the PIC simulations Table 1 shows the time averaged standard deviation of the  $E_r$  for different time range.

After each resampling, the spurious oscillations grow slowly as can be seen between the resamplings at  $t = 6\tau_t$  and  $9\tau_t$ . However, in the initial period, the oscillation amplitude becomes large almost immediately so that by  $t \approx 3\tau_t$ , they reach the magnitude maintained throughout the non-resampled simulation. This is presumably due to the relatively rapid evolution of the system toward the equilibrium plasma flow, which would rapidly mix the particles in both configuration and velocity space. Apparently once the flow is near equilibrium, the mixing rates are more modest resulting in slower growth of the sampling errors and resulting oscillations. This suggests that rather than resampling at a fixed frequency, it would be useful to resample locally and adaptively based on local estimates of the sampling errors. This would be particularly useful in simulating transient phenomena, and could adaptively determine the required number of particles to attain a specified sampling error tolerance.

In PIC simulations, the primary computational cost is the evolution of particles, and the relative cost of periodic particle resampling in a plasma PIC simulation will be small. The primary expense in resampling is the setup and solution of the quadratic program. The dominant cost there is the QR factorization of the constraint matrix. This cost scales quadratically with the number of constraints. For the XGCa test case given above, this results in a computational complexity roughly 20 times that of a XGCa timestep (using an explicit RK4 time integrator). Given that the resampling occurs infrequently, in this case every 1500 steps, the resampling overhead is negligible (roughly 1% of the simulation cost). This computational complexity estimate over-estimates the relative cost of the resampling because it does not account for the cost of interprocess communication, which is important for the XGCa time advance but not resampling, because the resampling algorithm is completely local. Accurate timing data to more precisely characterize the cost impact of resampling in the context of XGCa requires full integration of the resampling algorithm into the XGCa software, which is currently being developed. The results presented here indicate that application of MPCR will allow significantly fewer particles to be used to attain the same accuracy, thereby reducing the cost of PIC simulations, which scale approximately with the number of particles.



Table 1: The time average standard deviation of  $E_r$  in Figure 10.

Time range	$\psi = 0.8$			$\psi = 0.5$			$\psi = 0.5$		
	500M*	50M**	50M+res***	500M	50M	50M+res	500M	50M	50M+res
$3 < t/\tau < 6$	2980	16400	2350	673	2600	699	380.61	1450	442.3
$6 < t/\tau < 9$	2660	17900	4690	711	2950	769	210.87	2210	342.71
$9 < t/\tau < 12$	4682	15100	5880	464.5	2230	714	400	1540	452.32

\*500 million particles.

\*\*50 million particles.

\*\*\*50 million particles with periodic resampling.

## 4 Summary and Conclusions

The MPCR (Moment Preserving Constrained Resampling) algorithm presented here is designed to reduce the sampling error introduced by particle representations of distribution functions in PIC simulations, while preserving important features of the distribution. The algorithm functions by first partitioning the particle phase space into bins. It then uses sampling techniques within each bin to generate new particle positions and velocities, and employs constrained optimization to adjust the particle weights in each bin to preserve essential moments of the distribution function. These can include such physically relevant quantities as mass, momentum, energy, current density and charge density. Further, for quantities that are projected onto the Eulerian grid in the PIC method, the preserved quantities include the projections onto each Eulerian degree of freedom. In this way, the Eulerian solution is unchanged by the resampling process. Finally, by performing the resampling in bins rather than globally, MPCR can be used to maintain the desired marker particle distribution and importance sampling weights, despite mixing and particle weight evolution due to the use of variance reduction sampling.

The quality and utility of the MPCR algorithm was demonstrated here through several examples. In application to a synthetic distribution and to particles extracted from the gyrokinetic plasma PIC code XGC1, MPCR was shown to preserve extraordinary features of the distribution and to preserve various moments to the level or roundoff error. Using a neoclassical test problem, it was also shown that by periodic resampling using MPCR, the particle sampling error can be significantly reduced, to a level comparable to a simulation with an order of magnitude more particles. Further, the computational cost of the periodic resampling is negligible compared to the cost of the PIC simulation. Therefore, these tests indicate that the use of MPCR resampling in a PIC code can reduce computational cost and increase solution accuracy. While not pursued here, it was also noted that MPCR resampling can be applied locally and adaptively to ensure that sampling errors remain below specified tolerances.

## Acknowledgments

The work reported here was supported by the Department of Energy under grants de-sc0008454 and DE-AC02-09CH11466. The authors acknowledge the Texas Advanced Computing Center (TACC, <http://www.tacc.utexas.edu>) at The University of Texas at Austin as well as the National Energy Research Scientific Computing Center (NERSC, <http://www.nersc.gov>) and Oak Ridge Leadership Computing Facility (OLCF, <https://www.olcf.ornl.gov>) supported by U.S. Department of Energy Office of Science for providing HPC resources that have contributed to the research results reported here.

## References

- [1] Charles K Birdsall and A Bruce Langdon. *Plasma physics via computer simulation*. CRC Press, 2004.
- [2] Roger W Hockney and James W Eastwood. *Computer simulation using particles*. CRC Press, 1988.
- [3] TS Hahm. Nonlinear gyrokinetic equations for tokamak microturbulence. *Physics of Fluids (1958-1988)*, 31(9):2670–2673, 1988.
- [4] G.B. Jacobs and J.S. Hesthaven. High-order nodal discontinuous galerkin particle-in-cell method on unstructured grids. *Journal of Computational Physics*, 214(1):96 – 121, 2006.
- [5] A. Myers, P. Colella, and B. Van Straalen. A 4th-order particle-in-cell method with phase-space remapping for the vlasov–poisson equation. *SIAM Journal on Scientific Computing*, 39(3):B467–B485, 2017.
- [6] Thomas Westermann. Numerical modelling of the stationary maxwell–lorentz system in technical devices. *International Journal of Numerical Modelling: Electronic Networks, Devices and Fields*, 7(1):43–67, 1994.
- [7] F. Hermeline, S. Layouni, and P. Omnes. A finite volume method for the approximation of maxwells equations in two space dimensions on arbitrary meshes. *Journal of Computational Physics*, 227(22):9365 – 9388, 2008.
- [8] F. Assous, P. Degond, E. Heintze, P.A. Raviart, and J. Segre. On a finite-element method for solving the three-dimensional maxwell equations. *Journal of Computational Physics*, 109(2):222 – 237, 1993.
- [9] J Bao, Z Lin, A Kuley, and ZX Wang. Nonlinear electromagnetic formulation for particle-in-cell simulation of lower hybrid waves in toroidal geometry. *Physics of Plasmas*, 23(6):062501, 2016.
- [10] Ahmet Y Aydemir. A unified Monte Carlo interpretation of particle simulations and applications to non-neutral plasmas. *Physics of Plasmas (1994-present)*, 1(4):822–831, 1994.
- [11] R. Kleiber, R. Hatzky, A. Knies, K. Kauffmann, and P. Helander. An improved control-variate scheme for particle-in-cell simulations with collisions. *Computer Physics Communications*, 182(4):1005 – 1012, 2011.
- [12] Roman Hatzky, Axel Könies, and Alexey Mishchenko. Electromagnetic gyrokinetic PIC simulation with an adjustable control variates method. *Journal of Computational Physics*, 225(1):568–590, 2007.

- [13] Eric Sonnendrücker, Abigail Wachter, Roman Hatzky, and Ralf Kleiber. A split control variate scheme for PIC simulations with collisions. *Journal of Computational Physics*, 295:402–419, 2015.
- [14] Neil J Gordon, David J Salmond, and Adrian FM Smith. Novel approach to nonlinear/non-gaussian bayesian state estimation. In *IEE Proceedings F-Radar and Signal Processing*, volume 140, pages 107–113. IET, 1993.
- [15] Genshiro Kitagawa. A Monte Carlo filtering and smoothing method for non-gaussian nonlinear state space models. In *Proceedings of the 2nd US-Japan joint seminar on statistical time series analysis*, pages 110–131, 1993.
- [16] Genshiro Kitagawa. Monte Carlo filter and smoother for non-gaussian nonlinear state space models. *Journal of computational and graphical statistics*, 5(1):1–25, 1996.
- [17] Randal Douc and Olivier Cappé. Comparison of resampling schemes for particle filtering. In *Image and Signal Processing and Analysis, 2005. ISPA 2005. Proceedings of the 4th International Symposium on*, pages 64–69. IEEE, 2005.
- [18] Mark R Morelande and Alan M Zhang. A mode preserving particle filter. In *Acoustics, Speech and Signal Processing (ICASSP), 2011 IEEE International Conference on*, pages 3984–3987. IEEE, 2011.
- [19] Gregory L Eyink and Sangil Kim. A maximum entropy method for particle filtering. *Journal of statistical physics*, 123(5):1071–1128, 2006.
- [20] Yohan Petetin and François Desbouvries. Optimal sir algorithm vs. fully adapted auxiliary particle filter: a non asymptotic analysis. *Statistics and computing*, 23(6):759–775, 2013.
- [21] Giovanni Lapenta and Jeremiah U. Brackbill. Dynamic and selective control of the number of particles in kinetic plasma simulations. *Journal of Computational Physics*, 115(1):213 – 227, 1994.
- [22] Giovanni Lapenta. Particle rezoning for multidimensional kinetic particle-in-cell simulations. *Journal of Computational Physics*, 181(1):317 – 337, 2002.
- [23] Giovanni Lapenta and JU Brackbill. Control of the number of particles in fluid and mhd particle in cell methods. *Computer physics communications*, 87(1-2):139–154, 1995.
- [24] Jannis Teunissen and Ute Ebert. Controlling the weights of simulation particles: adaptive particle management using k-d trees. *Journal of Computational Physics*, 259:318 – 330, 2014.

- [25] M. Vranic, T. Grismayer, J.L. Martins, R.A. Fonseca, and L.O. Silva. Particle merging algorithm for PIC codes. *Computer Physics Communications*, 191:65 – 73, 2015.
- [26] F. Assous, T. Pougeard Dulimbert, and J. Segre. A new method for coalescing particles in PIC codes. *Journal of Computational Physics*, 187(2):550 – 571, 2003.
- [27] D.R. Welch, T.C. Genoni, R.E. Clark, and D.V. Rose. Adaptive particle management in a particle-in-cell code. *Journal of Computational Physics*, 227(1):143 – 155, 2007.
- [28] Phuc T. Luu, T. Tckmantel, and A. Pukhov. Voronoi particle merging algorithm for PIC codes. *Computer Physics Communications*, 202:165 – 174, 2016.
- [29] M. Pfeiffer, A. Mirza, C.-D. Munz, and S. Fasoulas. Two statistical particle split and merge methods for particle-in-cell codes. *Computer Physics Communications*, 191:9 – 24, 2015.
- [30] S. Ku, C.S. Chang, and P.H. Diamond. Full-f gyrokinetic particle simulation of centrally heated global itg turbulence from magnetic axis to edge pedestal top in a realistic tokamak geometry. *Nuclear Fusion*, 49(11):115021, 2009.
- [31] S. Ku, C.S. Chang, and P.H. Diamond. Full-f gyrokinetic particle simulation of centrally heated global ITG turbulence from magnetic axis to edge pedestal top in a realistic tokamak geometry. *Nucl. Fusion*, 49(11):115021, 2009.
- [32] Chak-Kuen Wong and Malcolm C. Easton. An efficient method for weighted sampling without replacement. *SIAM Journal on Computing*, 9(1):111–113, 1980.
- [33] Charles L Lawson, 1938 Hanson, Richard J., Society for Industrial, and Applied Mathematics. *Solving least squares problems*. Philadelphia : SIAM, [rev. ed.] edition, 1995. "This SIAM edition is an unabridged, revised republication of the work first published by Prentice-Hall, Inc., Englewood Cliffs, New Jersey, 1974"–T.p. verso.
- [34] Kristopher R Beevers and Wesley H Huang. Fixed-lag sampling strategies for particle filtering slam. In *Robotics and Automation, 2007 IEEE International Conference on*, pages 2433–2438. IEEE, 2007.
- [35] AN Timokhin. Time-dependent pair cascades in magnetospheres of neutron stars–i. dynamics of the polar cap cascade with no particle supply from the neutron star surface. *Monthly Notices of the Royal Astronomical Society*, 408(4):2092–2114, 2010.
- [36] EN Nerush, I Yu Kostyukov, AM Fedotov, NB Narozhny, NV Elkina, and H Ruhl. Laser field absorption in self-generated electron-positron pair plasma. *Physical review letters*, 106(3):035001, 2011.

- [37] S. Ku, C. S. Chang, R. Hager, R. M. Churchill, G. R. Tynan, I. Cziegler, M. Greenwald, J. Hughes, S. E. Parker, M. F. Adams, E. D’Azevedo, and P. Worley. A fast low-to-high confinement mode bifurcation dynamics in the boundary-plasma gyrokinetic code XGC1. *Physics of Plasmas*, 25(5):056107, 2018.
- [38] C. S. Chang, S. Ku, P. H. Diamond, Z. Lin, S. Parker, T. S. Hahm, and N. Samatova. Compressed ion temperature gradient turbulence in diverted tokamak edge. *Physics of Plasmas*, 16(5):056108, 2009.
- [39] J. Wesson and D.J. Campbell. *Tokamaks*. International Series of Monographs on Physics. OUP Oxford, 2011.
- [40] S. Ku, R. Hager, C.S. Chang, J.M. Kwon, and S.E. Parker. A new hybrid-lagrangian numerical scheme for gyrokinetic simulation of tokamak edge plasma. *Journal of Computational Physics*, 315:467 – 475, 2016.
- [41] Mark F Adams, Seung-Hoe Ku, Patrick Worley, Ed D’Azevedo, Julian C Cummings, and CS Chang. Scaling to 150k cores: recent algorithm and performance engineering developments enabling xgc1 to run at scale. In *Journal of Physics: Conference Series*, volume 180, page 012036. IOP Publishing, 2009.
- [42] Rex A. Dwyer. Higher-dimensional voronoi diagrams in linear expected time. *Discrete & Computational Geometry*, 6(3):343–367, 1991.
- [43] Donald Goldfarb and Ashok Idnani. A numerically stable dual method for solving strictly convex quadratic programs. *Mathematical programming*, 27(1):1–33, 1983.
- [44] A.T. Berwin. quadprog, a FORTRAN library for solving quadratic programming problems. <https://github.com/badgerodon/quadprog>, 2013.
- [45] R. Hager and C. S. Chang. Gyrokinetic neoclassical study of the bootstrap current in the tokamak edge pedestal with fully non-linear coulomb collisions. *Phys. Plasmas*, 23(4):042503, 2016.
- [46] S Ku, R Hager, CS Chang, JM Kwon, and SE Parker. A new hybrid-lagrangian numerical scheme for gyrokinetic simulation of tokamak edge plasma. *J. Comput. Phys.*, 315:467–475, 2016.